Sedimentary Geology 386 (2019) 118–131

Contents lists available at ScienceDirect

Sedimentary Geology

journal homepage: www.elsevier.com/locate/sedgeo

Elemental geochemistry to complement stable isotope data of fossil travertine: Importance of digestion method and statistics

Hannes Claes [a,b,*], Marijke Huysmans [c], Jeroen Soete [a], Katrijn Dirix [a,d], Elvira Vassilieva [a], Marcelle Marques Erthal [a,e], Wim Vandewijngaerde [a], Helen Hamaekers [a,f], Cihan Aratman [a,g], Mehmet Özkul [g], Rudy Swennen [a,**]

[a] Geodynamics and Geofluids Research Group, Department of Earth and Environmental Sciences, KU Leuven, Celestijnenlaan 200E, B-3001 Leuven, Belgium
[b] Clay and Interface Mineralogy (CIM), Bunsenstrasse 8, RWTH Aachen University, 52072 Aachen, Germany
[c] Hydrology and Hydraulic Engineering, Vrije Universiteit Brussel, Pleinlaan 2, 1050 Brussel, Belgium
[d] VITO, Flemish Institute for Technological Research, Boeretang 200, 2400 Mol, Belgium
[e] Petrobras Research Center, Av. Horácio de Macedo Cidade Universitária, 950, Ilha do Fundão, Rio de Janeiro 21941-915, Brazil
[f] SCR Sibelco nv, Department of Geology, De Zate 1, BE-2480 Dessel, Belgium
[g] Department of Geological Engineering, Pamukkale University, 20070 Kınıklı Campus, Denizli, Turkey

ARTICLE INFO

Article history:
Received 4 February 2019
Received in revised form 4 April 2019
Accepted 5 April 2019
Available online 13 April 2019

Editor: Dr. B. Jones

Keywords:
Travertines
Geochemistry
Statistics
Multivariate analyses
Major and trace elements
Stable isotopes

ABSTRACT

Elemental data from travertines are a treasure of depositional and diagenetic information. However, correct interpretation requires proper data acquisition and treatment. This study shows how results from elemental analyses complement sedimentological and other geochemical, i.e. isotopic, data and thereby contribute to our understanding of fossil travertines. Multivariate statistical element analyses, after multiple travertine digestion methods, demonstrate the link between elements, their mineralogical phases, and ultimately their origin. This study reveals that carbonate-phase related elements in travertines (Sr, S, Ba, Mg and Na) originate dominantly from the fluid source rocks. In combination with the $\delta^{18}O$ and $\delta^{13}C$ signatures, they are thus key geochemical variables for comparison of different travertine geobodies. Geochemical data analysis (elemental concentrations and isotope signatures), as illustrated here for the Turkish Ballık travertines, supports interpretation with regard to fluid source rock, distance from the vent and relative intensity of processes like evaporation and degassing. For fossil travertines, geochemical data can thus provide crucial insights for understanding the hydrologic system. In particular when information is restricted to borehole data, like in subsurface reservoirs, their application could be decisive.

1. Introduction

Spring-related continental carbonates precipitate from supersaturated spring waters, mainly due to CO_2 degassing. Two main groups are distinguished based on the origin of the water: Hydrothermal springs are associated with "travertines", while precipitates from lower temperature karstic waters with more macro-biotic influence are considered "calcareous tufa" (e.g. Pedley, 1990; Ford and Pedley, 1996). For fossil deposits the temperature and origin of the water can be more difficult to deduce. Capezzuoli et al. (2014) distinguished typical "travertine" from "tufa" fabrics. These authors recognised the continuity between the two endmembers and introduced the term "travitufa". For fossil deposits, premature conclusions on classification can be avoided by applying the term travertine sensu lato (s.l.) (Pentecost, 2005), thus incorporating both travertine (s.s.) and tufa. It is in this way that the term travertine is applied in this study. Distinction can be made based on the source of CO_2, as commonly deduced from stable isotope signatures. For meteogene/epigenic/epigean travertines, the CO_2 has a meteoric origin (vegetation, soil and atmosphere), while for a contribution of CO_2 from a deep, thermal origin, travertines are considered as being thermogene/endogenic/hypogean (Pentecost, 2005/Crossey et al., 2006/Teboul et al., 2016; respectively). A more elaborate discussion on terminology can be found in Pentecost (2005), Capezzuoli et al. (2014), Claes et al. (2015) and Della Porta (2015).

Recently there has been growing interest in travertines because of their potential application as hydrocarbon reservoir analogues (e.g. Ronchi and Cruciani, 2015; Claes et al., 2017a) and as palaeoclimate

* Correspondence to: H. Claes, Clay and Interface Mineralogy (CIM), Bunsenstrasse 8, RWTH Aachen University, 52072 Aachen, Germany.
** Correspondence to: R. Swennen, Geodynamics and Geofluids Research Group, Department of Earth and Environmental Sciences, KU Leuven, Celestijnenlaan 200E, B-3001 Leuven, Belgium.
E-mail addresses: hannes.claes@emr.rwth-aachen.de (H. Claes), rudy.swennen@kuleuven.be (R. Swennen).

https://doi.org/10.1016/j.sedgeo.2019.04.002
0037-0738/

archives (e.g. Ihlenfeld et al., 2003; Garnett et al., 2004; Fairchild and Treble, 2009; Yan et al., 2012; Wang et al., 2014), for example attesting CO_2 leakage (e.g. Kampman et al., 2012). Several studies prove the application of combined sedimentological-geochemical studies in understanding travertine 3D geobody architecture, the hydrologic system and diagenesis (e.g. Croci et al., 2016; Claes et al., 2017b; Frery et al., 2017; Rodríguez-Berriguete et al., 2017; Török et al., 2017, Mohammadi et al., 2019). However, the geochemical data of these studies are limited to stable and radiogenic isotope data. Despite their potential, studies on major and trace element concentrations in travertines are virtually lacking (cf. Teboul et al., 2016). Studies that do incorporate elemental analyses, often tend to focus on the water element content in active systems (e.g. Minissale et al., 2002; Crossey et al., 2006; Renaut et al., 2013). For fossil systems, most studies in literature only exploit a specific element or a narrow band of the full elemental spectrum (e.g. Cidu et al., 1990; Garnett et al., 2004; Sant'Anna et al., 2004: Bonny and Jones, 2008). Few studies have assembled a larger multi-element dataset (e.g. Pentecost, 1993, 1999; Pisarskii et al., 1998; Fouke et al., 2000; Kallis et al., 2000; Mallick and Frank, 2002; D'Alessandro et al., 2007; Kele et al., 2008, 2011; Gradzinski et al., 2013; Özkul et al., 2013; Asta et al., 2017) but do not statistically appreciate their datasets. Pavlovic et al. (2002), Leybourne et al. (2009) and Arenas et al. (2010) did analyse their datasets by multivariate analyses. Elements resulting from detrital phases, however, are discussed together with elements from the carbonate phase. Furthermore, the element compositions reported throughout the literature correspond to variable, often weak acid, dissolution/digestion and different measurement methods (see overview in Annex 1). These methods have differing extents of digestion and thus a different contribution of (mainly) detrital phases. In review books (e.g. Pentecost, 2005) all these results are discussed together, without separation of the data according to the applied dissolution/digestion methodology. A major advancement recently has been made by Teboul et al. (2016), who combined results from proper analyses with literature. They were able to deduce specific elements, like Ba and Sr, which can be used in discriminating the rock lithologies prevailing in the hydrogeological or palaeo-hydrogeological setting. The reasons why these elements are more useful in comparison to others, and how these elements can provide information within a site, unfortunately were not addressed.

Consequently, this study reaches beyond filling the gap of travertine elemental data but aims to answer the following research questions:

- What is the impact of the digestion method on the measured elemental concentrations? And which method is recommended?
- Which elements can be used best for comparison between different travertine bodies? What are the chemical reasons behind these recorded signatures?
- Are the elemental signatures mainly related to the parental fluids, the depositional environment (i.e. lithofacies), the distance from the spring and/or the diagenetic alterations?

To address these research questions multivariate analyses are introduced here for fossil travertine research. The goal is to fully appreciate large datasets and to capture the parameter variability.

2. Geological setting of the Ballık area case study

As a case study, travertines from the Ballık area (Denizli, SW Turkey) were sampled. The area lies on the northern edge of the Denizli basin, which is known for its numerous travertine occurrences (Fig. 1). The best example is the world heritage site of Pamukkale (Fig. 1; Kele et al., 2011). Özkul et al. (2013) provided a recent overview of the travertine occurrences in the Denizli basin, including U-series and thermoluminescence (TL) dating. The Ballık area is the largest and oldest travertine site in the Denizli basin, with an estimated volume of 0.94 km^3 over an area of ~4.8 × ~2.8 km^2 (Özkul et al., 2013; Pleistocene age >1.07 Ma cfr. Lebatard et al., 2014). Five key quarries (Ece, Faber, Çakmak, Ilık and Alimoğlu) that are part of the Killik dome in the Ballık area were selected for this study (Fig. 2). The study benefits from earlier sedimentological, diagenetic and isotope geochemical data of travertines from the Ece, Faber and Çakmak quarries (Claes et al., 2015; El Desouky et al., 2015; De Boever et al., 2017; Claes et al., 2017a; Mohammadi et al., 2019). The dataset is now enlarged with additional sedimentological mapping of the travertines from Çakmak, Ilık and Alimoğlu (Fig. 2), extra stable isotope analyses of samples from the Ilık and Alimoğlu travertines, and elemental characterisation of samples from all five quarries. The exposed travertine in the quarries reaches a thickness of >60 m. Based on a recent core, at least 60 m of additional travertines below the Faber quarry is proven (unpublished internal report, TraRAS project). The Killik dome area is ~1.3 by ~0.8 km^2 (Fig. 2). The environment of precipitation evolved from dominantly subaqueous in a water column to precipitation in a thin waterfilm, as represented by the sub-horizontal and biostromal reed facies and the cascade, waterfall and biohermal reed facies, respectively (Claes et al., 2015). More information on the geological setting, the sedimentology, fluid system and the structural context of the Ballık area can be found in Van Noten et al. (2013, 2019), El Desouky et al. (2015), Claes et al. (2015), De Boever et al. (2017) and Mohammadi et al., 2019. Additional data on their petrophysical properties (porosity, permeability, acoustic properties, …) can be found in Soete et al. (2015), De Boever et al. (2016) and Claes et al. (2017a).

3. Methods

3.1. Field mapping and sampling

Detailed photographs of all the quarry walls of the different excavation levels were printed and used in the field as background pictures for detailed line-drawings of the lithofacies. Hand samples were collected along, in total, 9 semi-continuous vertical sections, in analogy to boreholes in subsurface reservoirs. Three samples were collected per excavation level, which resulted in a vertical sample density of one sample every 2–3 m, or about 50 samples in each of the 5 quarries.

Based on the detailed drawings of the quarry walls and on the sampled sections, an overall 3D geobody facies distribution has been constructed. To gain better insight into the spatial distribution of the facies, based on the line drawings the facies were projected on the quarry walls using 3D drawing software (SketchUp Make, Trimble Incorporate, Sunnyvale, California), as shown in Fig. 2.

3.2. Trace element analyses

Homogenized bulk samples were measured using Inductively Coupled Plasma – Optical Emission Spectroscopy (ICP-OES). This approach has the advantage of measuring multiple elements relatively fast and simultaneously for large sample sets. ICP-OES is a wet analytical method, which requires the rock samples to be dissolved in acid.

Representative ~1 cm^3 pieces were cut from the samples, avoiding weathered or altered zones of the sample. Sample representativity was assured by petrographical thin-section analyses. After drying, powdering and physical mixing using a ceramic mortar (DIN EN 60672 C 110) and a tungsten carbide micro-mill, three different acid combinations were tested, i.e. a 1 acid digestion (HCl), 2 acid digestion (HCl and HNO_3) and 4 acid digestion (HNO_3, $HClO_4$, HF, HCl) method (Detailed description in annex). For the digested samples of all three methods, a Varian 720-ES instrument (Varian Medical Systems, Incorporated, Palo Alto, California, U.S.A.) supplied with double-pass glass cyclonic spray chamber, concentric glass nebulizer SeaSpray and an "extended high solids" torch was used to determine the concentrations of the following 23 elements: Al, As, Ba, Ca, Co, Cr, Cu, Fe, K, Li, Mg, Mn, Na, Ni, P, Pb, Rb, S, Si, Sr, Ti, V and Zn (Further details on methodology in annex).

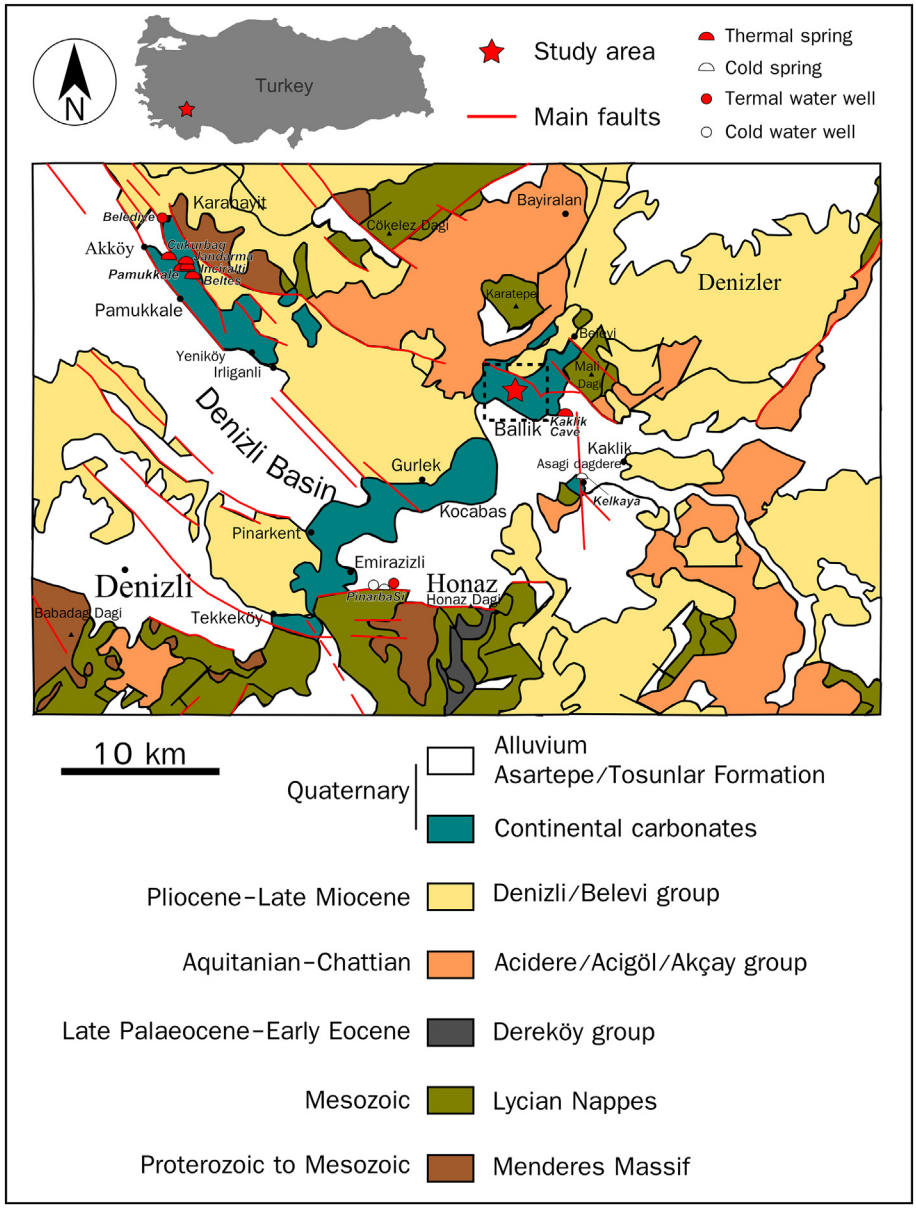

Fig. 1. Geological map of the Denizli basin (from Claes et al., 2015). Striped rectangle, about in the middle of the figure, indicates the location of Fig. 2A. Locations of wells and springs from Özkul et al. (2013).

There are some inherent differences to the methods of digestion that need to be considered. Weaker acids at lower temperature will not or only partly attack chemically more stable minerals, like silicates (e.g. Gleyzes et al., 2002). 1 M HCl is the most intuitive limestone digestion method since it is applied in mineralogy to differentiate calcite and dolomite from other minerals. Carbonates will dissolve. However, partly dissolved oxy-hydroxides and elements adsorbed to the surfaces of clays and organic matter will also contribute to the elemental concentrations. For the 2 acid method HCl is combined with HNO_3, which is a powerful solvent for sulphides, phosphates and organic matter. The 4 acid method completely dissolves the clays. Besides HCl and HNO_3, the latter method also uses $HClO_4$ and HF. $HClO_4$ is a very powerful oxidizing and dehydrating agent. It has a high boiling point and replaces other acids in their salts. HF reacts with silicates to form the very unstable volatile silicon tetra-fluoride SiF_4 (consequently it is not possible to determine Si concentration for 4 acid method). At the end 1 M HCl is used again as a leach. In summary, especially the contribution of non-carbonate phases to the elemental concentrations is expected to depend on the acid strength and the duration of the reaction.

3.3. Multivariate statistics on trace elements

The data were statistically analysed using R software (R core Team, 2013). Several standard statistical functions are, however, only applicable to unconstrained, normally distributed data. This assumption generally does not hold for geochemical data since they are expressed as relative values (% or ppm). The geochemical data are "closed" (Aitchison, 1986). Therefore, prior to the multivariate analysis, element concentration values were transformed. For compositional data, both centred log ratio (CLR; Aitchison, 1986) and isometric log ratio (ILR; Egozcue et al., 2003) transformations are common. Correlation between the transformed data cannot be interpreted as correlations between the original variables (e.g. Filzmoser and Hron, 2009). In order to establish which elements are linked by the same process or origin, elemental Ward hierarchical

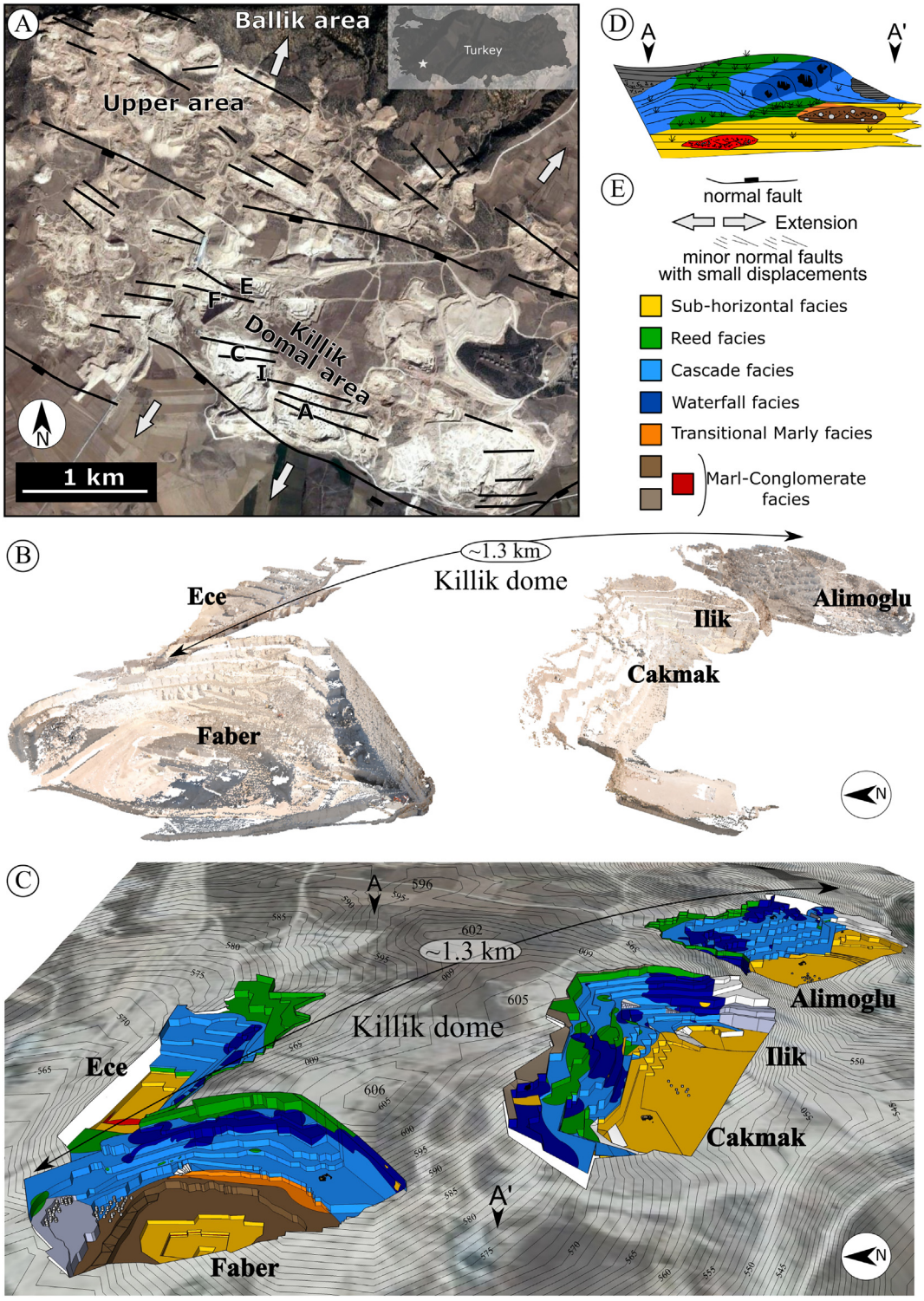

Fig. 2. (A) Overview of the Ballık area, with the five quarries included in this study indicated: Ece (E), Faber (F), Çakmak (C), Ilık (I) and Alimoğlu (A). Map modified from Google Earth, after Claes et al. (2015). (B) Overview of LiDaR scanned quarries inside the Killik dome. (C) Overview of the lithofacies mapped on the quarry walls of the quarries of the Killik dome inside the topography (from Google Earth), constructed in SketchUp Make (Trimble). (D) Schematic representation (not to scale) of the internal facies architecture along the A-A' transect indicated in C. (E) Legend. The faults shown in A are not indicated in (B) and (C).

cluster analyses and Principal Component Analyses (PCA) were executed. CLR preserves collinearity and thus the direct link to the variables. ILR avoids collinearity and gives more stable results for PCA (Filzmoser and Hron, 2009). For interpretation of the ILR PCA results, the data have to be back-transformed to the CLR space (Filzmoser et al., 2009). For each of the plots provided, it is explicitly stated which transformation and analyses have been performed. For further information on data treatment of the compositional data, the reader is referred to Van den Boogaert and Tolosano-Delgado (2013) and references therein.

3.4. Stable isotope analyses

Travertine subsamples for stable isotope analysis were obtained using a dental drill. Given the heterogeneous nature of travertines on

micro-scale, the most homogeneous parts of the rock framework were drilled. Cement samples were avoided for this study. Stable oxygen and carbon isotopic signatures of the samples were determined at the 'Friedrich-Alexander-Universität' (Erlangen-Nürnberg, Germany). Carbonate powders were reacted with 100% phosphoric acid at 70 °C in a Gasbench II connected to a ThermoFinnigan V+ mass spectrometer (Thermo Fisher Scientific Incorporated, Waltham, Massachusetts, U.S.A.). All values are reported in per mil (‰), relative to Vienna Pee Dee Belemnite (V-PDB) by assigning a $\delta^{13}C$ value of +1.95‰ and a $\delta^{18}O$ value of −2.20‰ to the standard NBS19. The analytical standard deviations for $\delta^{13}C$ and $\delta^{18}O$ are 0.04‰ and 0.05‰, respectively.

4. Results

4.1. Sedimentology

Four main travertine carbonate facies were identified, intercalated with more marly as well as conglomeratic facies. A short overview of the main facies characteristics is given below and in Figs. 2 and 3. A more detailed macroscopic and microscopic petrographic description can be found in Claes et al. (2015).

The mapped lithofacies (Fig. 2) show that an aggradational sub-horizontal or flat pool travertine facies (Fig. 3A) is present in the lower part of all quarries, extending at least 1500 by 500 m, with a minimal exposed thickness of 7 m. The sub-horizontal travertines are dominated by peloidal fabrics (Fig. 3E). From the Ece and Faber quarry towards the middle of the dome, in the Çakmak and Ilık quarry (Fig. 2), the occurrence of dendritic crusts in the sub-horizontal travertine facies increases. It is covered first by the biostromal reed facies (Fig. 3B) in the Ece quarry with locally more plant growth resulting in phyto-related fabrics (Fig. 3F). For the other quarries the sub-horizontal travertines are overlain by cascade (smooth slope and micro-terraced slope) travertines (Fig. 3C), characterised by dendritic crusts (Fig. 3C and G). The geobody vertically changes into a sloping system with first a gently crenulating, crinkly steady sloping cascade facies, evolving into a steeper sloping cascade facies and a strongly irregular steep sloping waterfall facies (Fig. 3D). Cascade travertines consist of isopachous beds, while the waterfall beds are anisopachous and even discontinuous, associated with primary cave development. The sloping facies are dominant in the Kıllık dome quarries (Fig. 2). The cascade facies, for example, extends over the entire dome, i.e. several km^2 in area, with a thickness of 15 to 30 m. Locally small pool facies were observed in between the cascade build-ups. In the central part of the Çakmak quarry and in the southeast of the Alimoğlu quarries patchily distributed decametre scale biohermal reed carbonates developed with lateral cascade and waterfall facies. Despite these complex morphologies, some clear systematic patterns exist. The general dip of the slopes from the cascade and waterfall facies is to the northwest in the Ece and Faber quarry. In the Çakmak quarry the slope direction tilts towards the west and eventually to the southwest in the Ilık quarry. In the Alimoğlu quarry the layers are dipping dominantly southwards, thus closing the domal structure (Fig. 2). The up to 20 m thick waterfall facies shows a pronounced prograding trend within the Ece, Faber and Çakmak quarry (Claes et al., 2015). On top of the waterfall facies, the decreasing steepness results again in the development of cascade facies. Reed facies subsequently levels up the domal deposits. The upper aggradational biostromal levelling up reed sequence has a lateral extension over >1000 m with a thickness ranging between 1 and 20 m. The travertine body is locally intercalated by lacustrine to palustrine varve-like marls, in which some high energy fluviatile conglomerates with imbricated clasts occur (Khatib et al., 2014; Claes et al., 2015). This is most pronounced as a maximally 17 m thick package in the Faber quarry, that

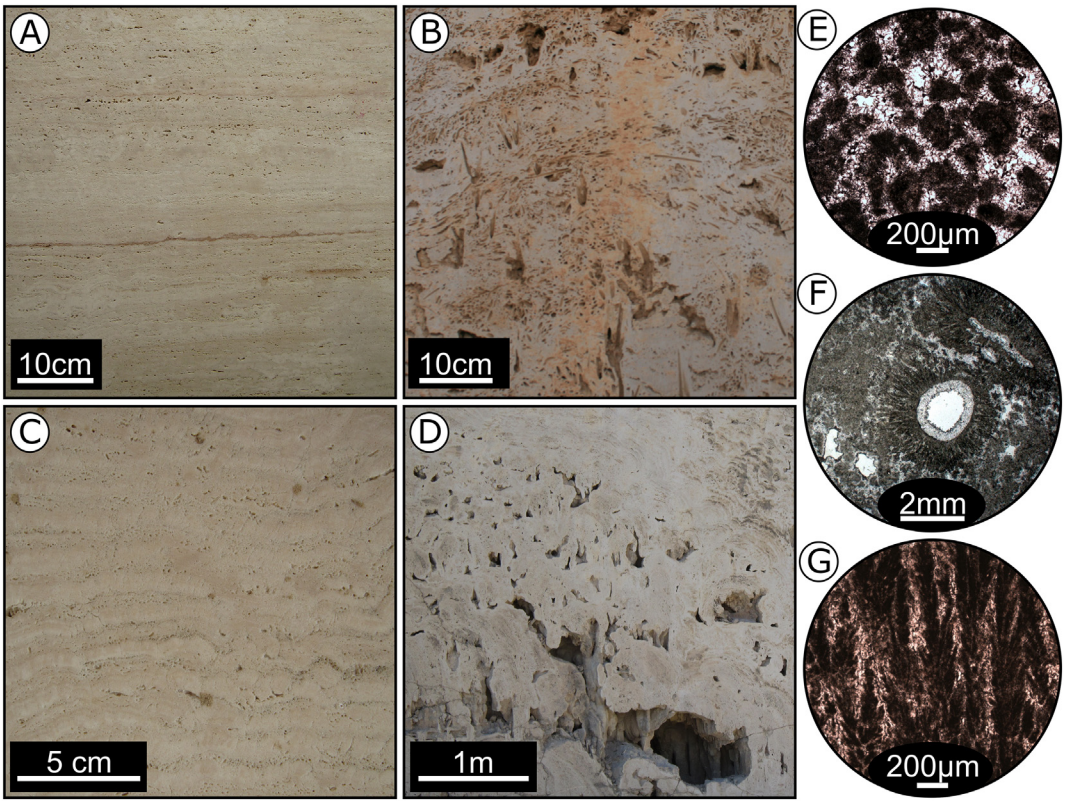

Fig. 3. Representative images of the four dominant travertine lithofacies with their dominant fabrics. (A) Sub-horizontal flat pool facies dominated by peloidal travertines with fenestral pores, and to less extent dendritic crusts. (B) Reed travertine facies dominated by phyto travertine fabrics with moulds of plants in growth and erosional position. (C) Cascade facies characterised by smooth sloping crusts of micritic dendrites, interlayered with peloidal travertines. (D) Waterfall facies characterised by its primary cavities, and dominated by phyto and dendrite crust travertines. (E) Microscopic image of peloidal travertine with peloidal micrite surrounded by spar crystals. (F) Microscopic image of phyto travertines with peloidal fabrics between encrusted reed moulds. (G) Microscopic image of undulating crusts consisting of micritic dendrites. (E–F) Modified from Claes et al. (2015).

Table 1
Results of the elemental analysis of a selected dataset ($n = 20$) from the Ece quarry, measured according to the three different digestion methods. Concentrations in μg/g.

Sample	Facies	1 Acid	2 Acid	4 Acid	1 Acid	2 Acid	4 Acid	1 Acid	2 Acid	4 Acid	1 Acid	2 Acid	4 Acid	1 Acid	2 Acid	4 Acid
		Al			Fe			Ba			Mg			Na		
EC10HC001	Sub-horizontal	14	18	27	27	35	34	7	9	9	1687	1831	2108	111	115	137
EC10HC003	Sub-horizontal	16	27	39	15	29	32	7	8	9	2137	2154	2548	78	136	159
EC10HC005	Sub-horizontal	9	17	4502	11	31	2660	7	7	27	1762	1750	3081	53	90	314
EC10HC006	Sub-horizontal	36	70	238	43	104	173	7	8	9	1745	1813	2185	46	104	137
EC10HC008	Reed	41	61	284	78	129	289	6	8	8	2055	2051	2470	69	121	160
EC10HC009	Cascade	47	83	207	41	96	143	7	8	9	2167	2113	2575	63	112	151
EC10HC010	Cascade	92	165	550	106	188	314	6	7	9	2199	2173	2650	56	111	170
EC10HC011	Cascade	42	81	165	37	85	120	9	11	12	1598	1695	2010	62	116	139
EC10HC012	Cascade	17	18	22	18	29	32	5	6	6	2009	2040	2449	73	100	133
EC10HC013	Cascade	8	24	43	8	32	43	4	7	7	1464	1928	2452	57	109	147
EC10HC016	Cascade	6	8	4	11	22	26	5	6	7	1730	1761	2225	39	88	124
EC10HC018	Cascade	14	18	52	16	31	48	6	6	8	1530	1601	2028	41	85	129
EC10HC019	Cascade	9	9	21	16	21	28	7	6	7	2077	1849	2293	61	91	137
EC10HC020	Waterfall	56	102	272	77	146	234	7	7	9	1885	1912	2419	61	106	156
EC10HC022	Waterfall	94	167	538	154	264	456	6	7	9	1712	1757	2212	56	80	152
EC10HC023	Waterfall	49	60	170	70	80	135	7	8	9	1542	1541	1969	64	72	143
EC10HC024	Waterfall	70	80	279	178	211	343	8	8	10	1453	1475	1903	40	69	135
EC10HC025	Waterfall	35	50	156	64	85	165	6	7	9	1381	1491	1859	56	75	146
EC10HC029	Reed	38	48	115	66	79	102	6	7	8	1383	1354	1867	43	61	126
Median		36	50	165	41	80	135	7	7	9	1730	1813	2225	57	100	143

quickly thins out over ~170 m to a thickness of ~8 m. Although this lithology reflects a high external input into the spring-fed system, transitional lithologies between travertines and marls were included in the sampling for both elemental as well as stable isotope analyses. Overlying sands and conglomerates were not included.

In line with the Ece, Faber and Çakmak quarries (Claes et al., 2015; El Desouky et al., 2015; Claes et al., 2017a; Mohammadi et al., 2019), early diagenetic fabrics were also commonly observed for samples from the Ilık and Alimoğlu quarries, e.g. the sparites in the peloidal travertines (Fig. 3E). Since these fabrics mainly result from syn-sedimentary fluids (e.g. El Desouky et al., 2015), the difference in geochemical signature of these early diagenetic with primary fabrics is small (e.g. Andrews and Brasier, 2005; Rainey and Jones, 2007; Claes et al., 2015). Macro-scale diagenetic alteration is limited and the depositional pore network is largely maintained. Angular crystal terminations point to a preservation of the original calcite mineralogy (Ross, 1991; Claes et al., 2017a). No aragonite was observed. In addition, of importance for the elemental analyses is that no salts, and only rarely a quartz grain was observed in the petrographic analyses. SEM observations reveal some clays, mainly in the marly lithologies intercalating the travertines.

4.2. Elemental data and their digestion method dependency

1 M HCl insoluble residue (quartz, clays and some organic matter) was never >11% (marl-conglomerate lithologies) and on average <5%. The 2 (and 4) acid residues were below the weight detection limit. In general, all elemental concentrations are the highest in the 4 acid method and the lowest in the 1 acid method (Table 1, and annex). The relative increase of the concentrations, from the 1 over 2 to 4 acid method, however, differs strongly for the different elements. Taking the recovery percentages into account between the 1 and 4 acid method, elements with a >60% increase on average include Al, Fe, K, Na and Ti. Elements like Mg, Mn and P differ on average by <30% and Ba, S and Sr by <20%. Ba, Mg, Mn, P, S and Sr are found to show practically no different concentrations between the 1 and 2 acid method. Surprisingly, Si concentrations (data in annex 3) are often higher in the 1 acid method compared to the 2 acid method results.

In order to deduce a common origin for the elements, PCA analyses were performed (Example in Fig. 4). The PCAs point out that the largest variability of the data (Component 1, >50%), is caused by the relative contribution of two opposing element groups. The relationship or alignment of the vertices of variables in the compositional PCA plot is governed by their relative covariance (e.g. Kynclova et al., 2016). Although the covariances of the ILR or CLR transformed data should not be interpreted as covariances of the untransformed data, they can be used as a distance measure for clustering. Ward hierarchical cluster dendrograms based on this relative covariance thus enable a grouping of the decisive elements (Fig. 5). Independent of the digestion method and clustering algorithm the same two groups are recognised. Group I with Ba, Mg, Na, S, and Sr can be distinguished from Group II containing Al, Fe, Si and Ti. The other elements show a weak or changing association in function of the applied digestion method with these main groups. This is most pronounced for K, which is strongly associated with Group I in the results from the 1 acid analysis and strongly associated with Group II for the 4 acid analysis. Mn and P show a weakened correlation with increasing acid strength.

These groups are very similar to the groups that were recognised for the acid-strength-related recovery percentages, at the beginning of this paragraph. The concentrations of Group I on the average differ by <30% for the different digestion methods, with the exception of sodium. The Sr concentrations for the 2 acid method on the average are only ~10% lower than the concentrations measured for the 4 acid digestion method. Elements related to Group II also tend to show higher imprecisions for the 1 acid and 2 acid digestion method (Appendix 1: Annex 2).

4.3. Stable carbon and oxygen isotopes

For the general cluster, so not taking statistical outliers into account, $\delta^{18}O$ ranges from about −9 to about −6‰ V-PDB (average −7.2‰ V-PDB), while $\delta^{13}C$ ranges from about −2 to about 3‰ V-PDB (average +0.5‰ V-PDB). The Ilık and Alimoğlu data, corresponding to the southernmost quarries, however, seem to be characterised by $\delta^{18}O$ and $\delta^{13}C$ signatures at the high end of the cluster. For the carbonates of these two quarries, $\delta^{18}O$ on average are −7.3 and −6.7‰ V-PDB respectively, while $\delta^{13}C$ are on average +0. 7 and +1.2‰ V-PDB. In particular $\delta^{13}C$ signatures also seem to show a decrease towards the top of the quarries.

4.4. Lithofacies dependency evaluation of the geochemical data

The elemental variation of the lithofacies depends largely on the lithology (Fig. 7). The elements of Group II are significantly higher for the marl-conglomerate facies then for the different travertine carbonate

1 Acid	2 Acid	4 Acid	1 Acid	2 Acid	4 Acid	1 Acid	2 Acid	4 Acid	1 Acid	2 Acid	4 Acid	1 Acid	2 Acid	4 Acid
S			Sr			K			Mn			P		
1003	1084	1247	280	740	784	77	25	22	2	3	3	15	15	31
1418	1423	1707	734	751	832	28	35	28	1	2	<2	19	19	40
1396	1382	1216	711	713	587	18	24	1129	2	2	25	23	23	90
1012	1044	1248	632	666	720	25	43	71	4	5	6	31	31	57
1401	1395	1633	524	537	604	30	40	80	18	18	26	38	36	59
1631	1583	1948	636	631	710	29	44	67	5	5	6	56	50	86
1369	1326	1637	559	564	630	42	64	156	4	5	7	35	33	57
1490	1546	1822	994	1064	1143	29	43	55	3	4	4	19	20	41
1564	1573	1895	546	568	620	25	28	23	2	3	3	20	20	38
1199	1592	1975	469	624	709	27	33	29	2	3	3	35	41	68
1230	1249	1536	549	570	642	14	27	19	2	2	3	28	27	48
1147	1199	1499	536	562	647	17	23	27	3	4	5	31	29	54
1562	1391	1696	724	655	736	25	26	24	4	4	5	34	30	50
1255	1267	1566	630	641	733	27	48	82	9	10	13	49	46	75
1049	1040	1291	684	687	775	35	56	140	24	25	33	80	74	111
1113	1087	1398	695	701	810	30	31	57	11	11	14	52	47	77
897	890	1150	531	529	626	29	36	84	9	9	12	57	54	89
955	1022	1273	666	709	798	21	26	50	20	21	28	99	95	137
663	639	1051	501	482	640	24	26	42	12	13	14	77	69	113
1230	1267	1536	630	641	710	27	33	55	4	5	6	35	33	59

lithofacies. The Group I elements are less influenced by this contrast and show some weak dependency and difference between the travertine lithofacies. Concentrations of S, Sr and Mg seem to be higher for the sub-horizontal and reed facies, with reed lithologies resulting in the highest values, in contrast to the cascade and waterfall facies. The waterfall facies often displays the lowest Group I element results. Sr seems to give the most distinct values for the travertine lithofacies. However, even for Sr, the elemental signatures of the lithofacies do not differ significantly (not even after transformation) and so not only the depositional environment but also other controlling factors need to be considered.

For the stable isotopes (also Fig. 7), the marl-conglomerate (carbonate matrix), cascade and sub-horizontal facies show a similar $\delta^{18}O$ signature, while that of the reed, and more pronounced the waterfall facies, show lower values. Only the difference of the waterfall facies is statistically significant on a 0.05 level. For $\delta^{13}C$, slightly more pronounced differences can be observed. Samples from sub-horizontal and reed facies show significantly higher and lower $\delta^{13}C$ values, respectively, compared to the other facies. It should be noted that the sub-horizontal travertines mostly occur in the lowest quarry parts and the reed facies mostly in the upper quarry parts.

5. Discussion

In order to evaluate how elemental data can complement sedimentological and other geochemical (e.g. isotopic) data in understanding fossil travertine systems, first a discussion on the element groups and an evaluation of the impact of the digestion method on the different element signatures are necessary. Consequently, this will first be discussed in paragraphs 5.1 and 5.2, followed by a conclusion on the optimal digestion method for an elemental comparison between travertines (Section 5.3). Subsequently, the proper elements of the dataset can be used, together with sedimentological and isotopic data, for interpretation towards their site-specific origin (Section 5.4) and processes controlling variation within sites (Section 5.5).

5.1. Carbonate (Group I) and non-carbonate related elements (Group II)

Independent of the digestion method, two main element groups can be distinguished for the travertines. Group I with Ba, Ca, Mg, S, Na and Sr can be related to the carbonate fraction of the samples, while Group II, containing Al, Fe, Si and Ti, can be related to the non-carbonate fraction (Salminen et al., 2006; Lovrenčić Mikelić et al., 2013; Fig. 5). Other elements show a weaker or changing association with the main groups and a stronger dependence of their concentration in function of the digestion method.

Elements can be incorporated in different sites in carbonates (Fairchild and Treble, 2009). Group I elements reflect on the one hand cations (such as Mg^{2+}, Sr^{2+} and Ba^{2+}) that can substitute Ca^{2+} in the calcite lattice and on the other hand the substitution of the sulphate anions (SO_4^{2-}) for the carbonate group (CO_3^{2-}). Sodium (Na^+) in the carbonate phase is usually located at the interstitial sites in the crystal lattice.

Group II elements are typically associated with non-carbonate phases. Aluminium, for example, is not incorporated in the calcite lattice and tends to correlate with iron in weathered material and alteration products of feldspar minerals, i.e. clays and oxi-hydroxides. Potassium is known to be associated with clays and is important in many plant metabolisms (e.g. Armengaud et al., 2009). The incorporation of manganese depends largely on its presence in the source rock and the redox conditions during transport and precipitation. Given the oxidizing conditions, the largest proportion is typically held in secondary Mn^{4+} oxides, that form either discrete concretions or surface coatings, or co-precipitates with Fe (oxi/hydroxides) (Salminen et al., 2006). Formation of iron and manganese oxides within the carbonates was locally observed in the field (Claes et al., 2015). Manganese less commonly results from detrital influx (Salminen et al., 2006). Noteworthy is that clays and Fe/Mn oxi/hydroxides often form aggregates in sedimentary systems. In sedimentary rocks, nickel is mostly held in detrital ferromagnesian silicate minerals, detrital primary Fe oxides, hydrous Fe and Mn oxides, and clay minerals (Salminen et al., 2006). In this case, weathering and erosion of the Lycian ophiolites in the hinterland (Alçiçek et al., 2007) can lead to the increase of Ni in the detrital material. A higher detrital input in the system is thus associated with elevated concentrations of Group II elements. Relatively major concentration differences of iron between the 1 and 2 acid method can be explained by the presence of iron oxides (Caboi et al., 1991). To a smaller extent, Group II elements can also be partly incorporated into the carbonates as submicrometre size colloids (=solid inclusions), aqueous inclusions and/or at defect sites in the crystals (Fairchild and Treble, 2009).

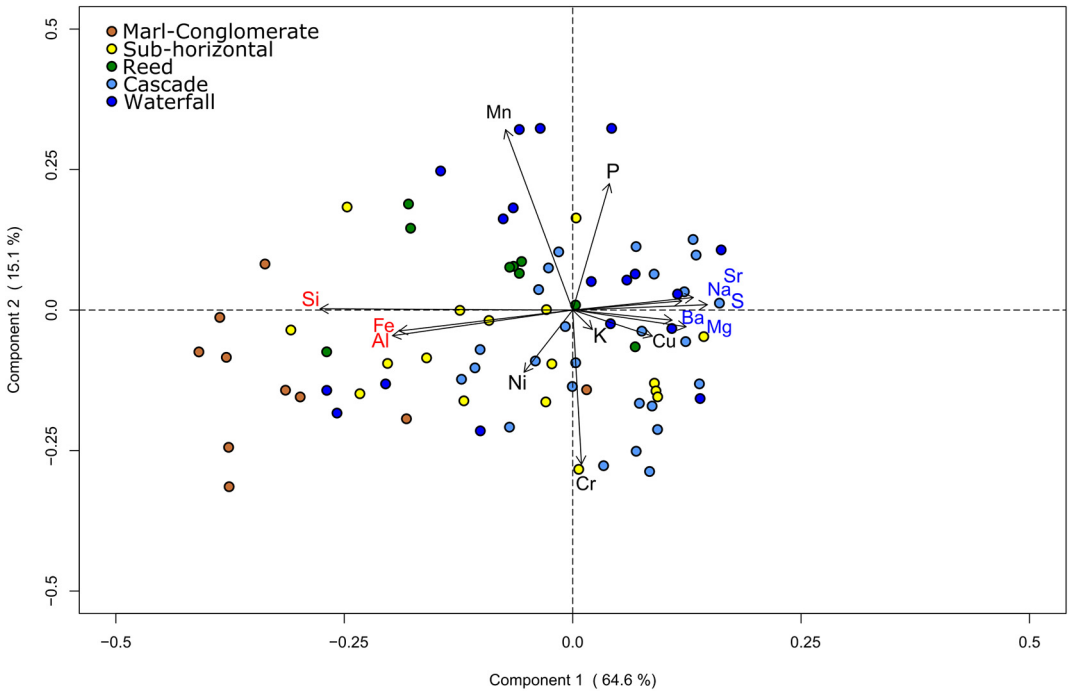

Fig. 4. Robust Principal Component Analysis plot of the two first components based on the ILR-transformed 1 acid dataset. Group II elements (Red) plot on the negative side of component 1, while Group I elements (Blue) plot on the positive side. (For interpretation of the references to colour in this figure legend, the reader is referred to the web version of this article.)

5.2. Digestion method dependency and elements with changing (strength of) group association

The influence of the non-carbonate fraction could be expected to be low for the almost purely calcitic travertines with a low non-carbonate fraction (<2 wt%; Soete et al., 2015). However, for carbonate research in general, the large extent to which the non-carbonate content controls litho-geochemical patterns has long been known (e.g. Swennen et al., 1986). Therefore, it is often opted to use a weak acid digestion or sequential extraction method in order to obtain geochemical information from the carbonates only. Even for the weak 1 acid method applied here, partly dissolved oxy-hydroxides and elements adsorbed to the surfaces of clays and organic matter contribute to the elemental patterns. In addition, the measured concentrations of non-carbonate related elements are less precise (see Annex 2). For weaker acids, often applied in sequential extraction procedures, these problems remain and additionally incomplete carbonate dissolution occurs (e.g. Gleyzes et al., 2002). Besides the laborious and time-consuming nature of sequential extraction procedures, there are also problems of non-selectivity of reagents and readsorption phenomena (Rendell et al., 1980; Howard and Vandenbrink, 1999).

By applying different digestion methods, however, it is possible to get more information on the association with the different speciation of some elements. The changing association of K from Group I to Group II in the weak to strong acid digestion, and the weakened correlation of Mn and P, with increasing acid strength, illustrate the multiple origins of these elements (Fig. 5). K partly relates to the carbonates, while the Mn—P association possibly could be related with the presence of traces of organic matter (Total Organic Content in general low, i.e. below 0.35%). When the non-carbonates are brought into solution due to the use of a stronger acid, the previous elemental concentrations are overruled by the non-carbonate input. Manganese, for example, is also known to be concentrated in erosional crusts and palaeosols (Salminen et al., 2006).

Aluminium can be taken as a representative element of Group II since it is most typically associated with the fine-grained detrital fraction. This is clearly reflected by its increase in concentration in the 2 acid, and even more in the 4 acid digestion results. A stronger acid digestion clearly increases the elemental concentrations for elements bound to the non-carbonate fraction, while those of the carbonate phase generally remain constant. A surprising exception is the silica concentration,

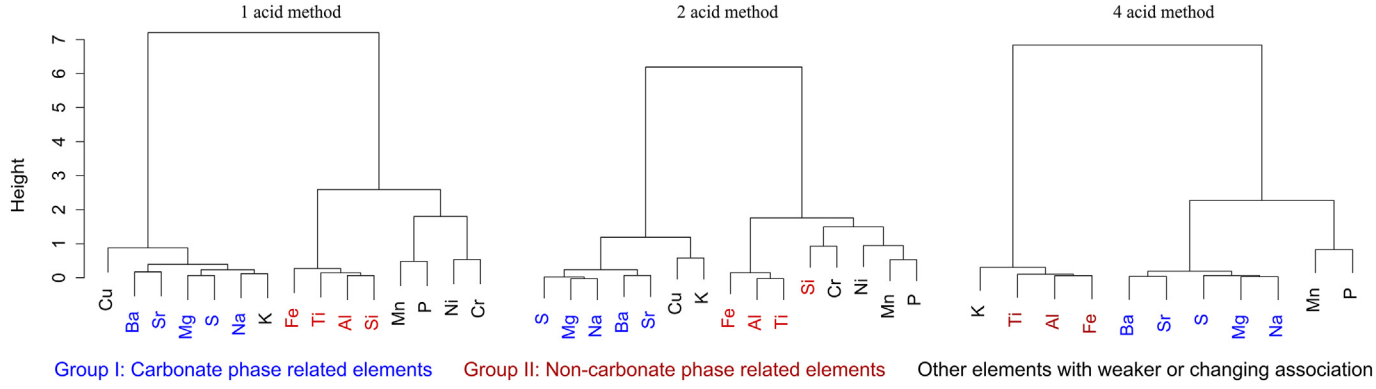

Fig. 5. Ward hierarchical cluster dendrograms of the CLR transformed data of Table 1. Loadings from the PCA are used as a distance measure. For all datasets similar clusters are obtained.

as it is lower for the 2 acid compared to the 1 acid results (Annex 3). This indicates extraction from the solution during the preparation of the measurement solutions, likely by flocculation. Also, even for the carbonate phase related elements, a (smaller) increase in elemental concentrations is observed with increasing acid strength. This can be explained by clay minerals that tend to coat carbonate grains and could protect them from dissolution (Rauch and White, 1977), also known as the "clay shielding effect".

5.3. Digestion methodology for comparison between travertine sites

For the trace elements, results of the incomplete digestion methods are highly dependent on the procedure used. Unless the element specific "offset" of the results with regard to a complete digestion is determined, this implies that they are unsuited for absolute geochemical comparison of most elements between travertine occurrences, and carbonates in general. Even when the same weak digestion acids are used, a standardisation is an absolute necessity since possibly factors like digestion time and temperature also can influence the extent of digestion, resulting in higher imprecisions. Complete digestion methods, like the applied 4 acid method, do enable an absolute comparison. Unfortunately, almost no complete digestion results of spring-related travertines are reported in literature. When applying complete digestion methods, elemental concentrations of clay-related elements will dominate the elemental spectrum in function of the external influx into the system. Although purely chemical separation of the different fractions is thus difficult, they can be deduced by statistics, emphasising the importance of data processing in geochemistry. The only way to evaluate geochemical differences related to deposition that remains is by statistical isolation of the carbonate fraction associated elemental concentrations (Group I), in this case Ba, Ca, Mg, Na, S and Sr.

5.4. Carbonate phase related elements (Group I) and stable and radiogenic isotopes as tracers of the fluid source rocks

Besides precipitation rate, the elemental concentrations in the water, and thus indirectly their availability in the stratigraphic column, will influence the carbonate element (Group I) concentration variation in the travertines. This is reported for example for Sr by Turi (1986), Irion and Müller (1968) and Pentecost (1993). In Italy, Minissale et al. (2002) reported on elevated and correlated concentrations of Sr and SO_4^{2-} in thermal springs, caused by the interaction of circulating groundwater with Triassic evaporitic bearing carbonates. Minissale (2004) was able to relate the progressive increase in Sr and S to spring temperature and to the length and depth of the hydrological circuits inside the Sr-rich anhydrite-bearing limestones. Teboul et al. (2016) also selected Ba and Sr as geochemical tracers to discriminate the source rocks of travertines. In conclusion, the carbonate-related elements (Group I), together with isotope results, are the most suited for comparison between travertine sites.

By comparison of the stable isotope data of this study with reported signatures from other studies (Fig. 6), it is clear that the Ballık signatures generally plot in the zone delineated for hypogean (Teboul et al., 2016), thermogene (Pentecost, 2005), or endogene (Crossey et al., 2006)

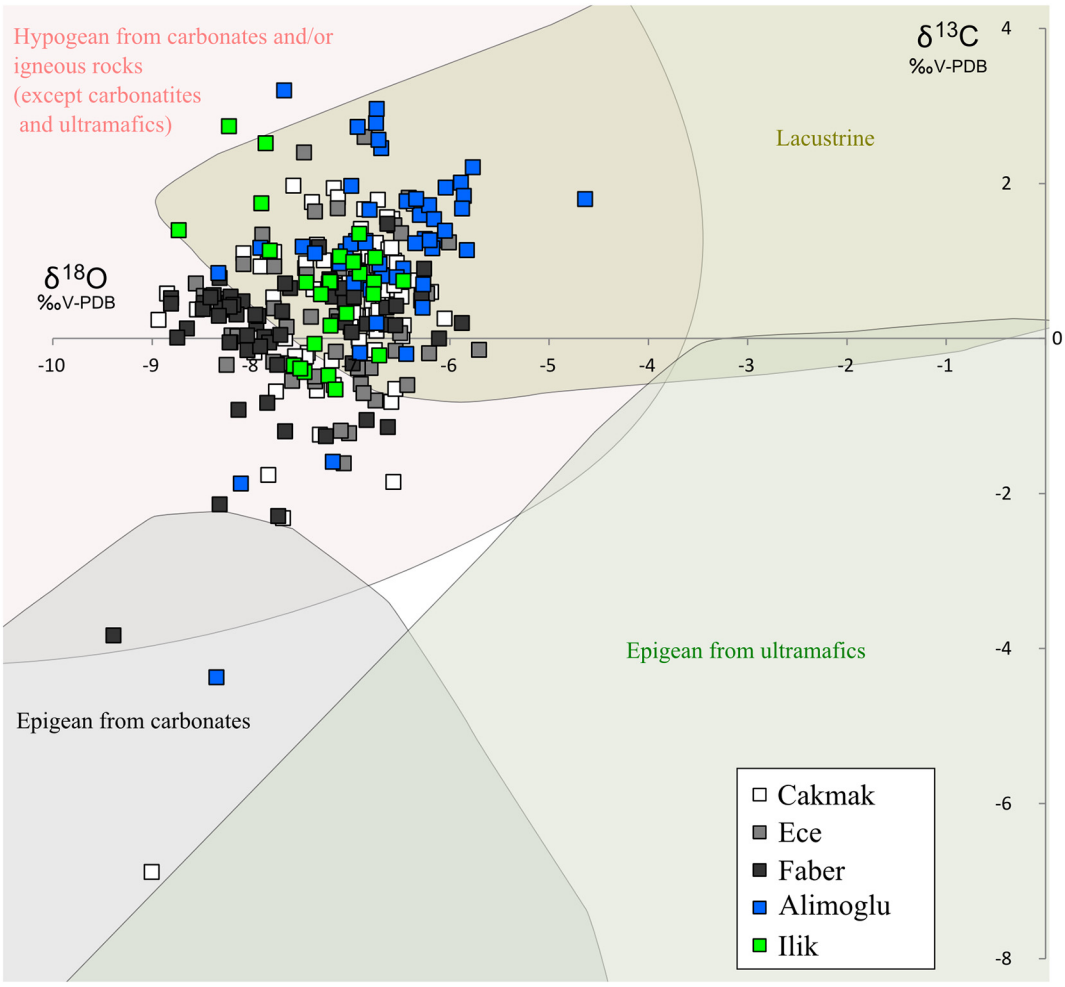

Fig. 6. $\delta^{18}O$ - $\delta^{13}C$ stable isotope plot of samples of the Killik dome according to sampling location (quarry name). Results from Ece and Faber from Claes et al. (2015) and for Çakmak from El Desouky et al. (2015). Source rock background regions based on Teboul et al. (2016).

travertines with carbonates and/or igneous rocks (except carbonatites and ultramafics) as source rocks (Teboul et al., 2016). The data of the Ballık area are in line with the low Ba (<100 ppm) and high Sr (>400 ppm) typical for source rocks consisting of mixed limestones, evaporites and dolomites. Stable carbon isotope signatures and strontium isotope ratios indicated the Lycian nappes as fluid source rocks for the Ballık travertines (Fig. 8; Claes et al., 2015; El Desouky et al., 2015). The reported relative quantities and covarying concentrations of Group I elements can be readily explained by interaction of deep fluids with their host rocks. The Triassic limestones from the Lycian nappes consist largely of dolomitic limestones (Alçiçek et al., 2007), possessing relatively high magnesium and highest sodium concentrations of all marine sedimentary rocks reported in the study area. The alternation of the dolomitic limestone with gypsum is typical for the Kaleboğazı Formation. Several nodules of calcite pseudomorphs after anhydrite and diagenetic sulphur minerals are observed in this

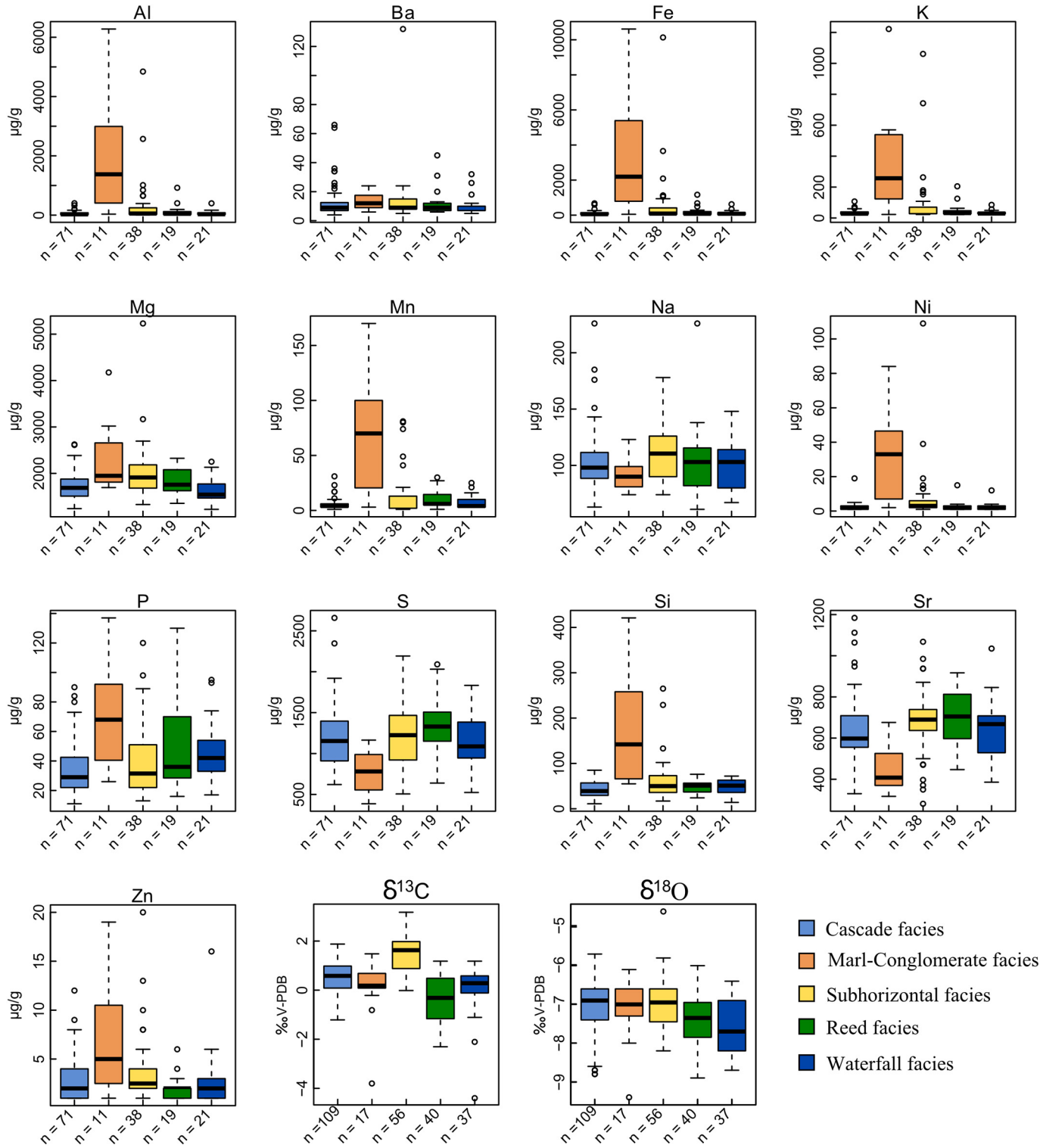

Fig. 7. Boxplots of samples of different lithofacies for different elements (2 acid sample set) and $\delta^{18}O$ and $\delta^{13}C$. Data are displayed as individual points when values are outside the range defined by [Q1–1.5 ∗ IQR, Q3 + 1.5 ∗ IQR]. With Q1 = 25% quartile, Q3 = 75% quartile, IQR = interquartile range.

formation (Gündoğan et al., 2008). The relatively elevated concentrations of Sr, S and Na can thus be related to the interaction of the fluids with the evaporites that are intercalated in the dolomitic limestone succession that is leached in the subsurface. Also the presence and concentration of barium is strongly controlled by its abundance in the bedrock.

Özkul et al. (2013) give an overview of elemental concentrations (among which Sr) related to hot springs in the Denizli basin. Elemental concentrations of the Ballık samples are among the lowest in the basin. The highest concentrations are reported for the Çukurbağ and Pamukkale sites (Fig. 1; Özkul et al., 2013). By comparison with local geology (e.g. Alçiçek et al., 2007; Simsek, 1984; Sun, 1990), rather than a temperature dependence, this seems related to the residence time and to the extent to which anhydrite-bearing limestone reservoirs are present in the subsurface, similar to Minissale (2004) in Italy. The variation of Sr values within the Ballık area, illustrates the geochemical variability over a relatively short (kilometre) distance. Rather than to the depositional environment (lithofacies), the basin-scale variation of the Group I elemental concentrations in spring-related travertines can be related to the fluid characteristics.

5.5. Geochemical spatial distribution within the Ballık travertine body

Element concentrations in source waters may vary through space, i.e. along the flow path (e.g. Kele et al., 2011), and time. In addition to these two controlling factors, elemental distribution can be overprinted by diagenesis. The superposition of these three controls potentially leads to complex elemental distributions. The variation within deposits, however, is much smaller than between sites, as illustrated by the uniformity in elemental signatures between the different lithofacies (Fig. 7). However, the elemental distributions, given their compositional nature, should be transformed (CLR or ILR) before interpretation. In addition, elemental data should be combined with stable isotope and sedimentological data.

The limited diagenetic alteration of the Ballık travertines and the relation of the geochemical parameters to the occurrence of the waterfall facies suggest a depositional scenario behind the geochemical data distributions. Even for travertines with more extensive (early) diagenetic

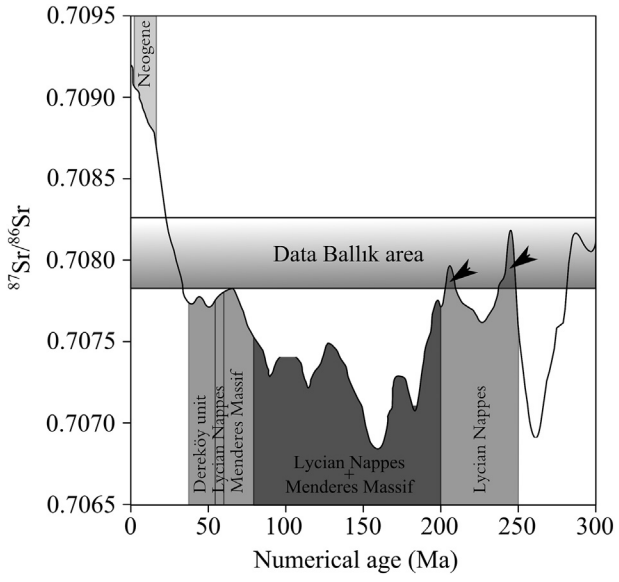

Fig. 8. The range of $^{87}Sr/^{86}Sr$ ratios of the travertine precipitates in the Ballık area (El Desouky et al., 2015; Claes et al., 2015) plotted in the marine $^{87}Sr/^{86}Sr$ curve through time (McArthur and Howarth, 2004), in comparison with the possible carbonate source rocks as deduced from the lithostratigraphy of the SW of the Denizli basin (Alçiçek et al., 2007; Claes et al., 2015). The arrows indicate the overlap between the data of the Ballık area and stratigraphic candidate fluid source rocks, highlighting the Lycian Nappes. Figure modified after El Desouky et al., 2015.

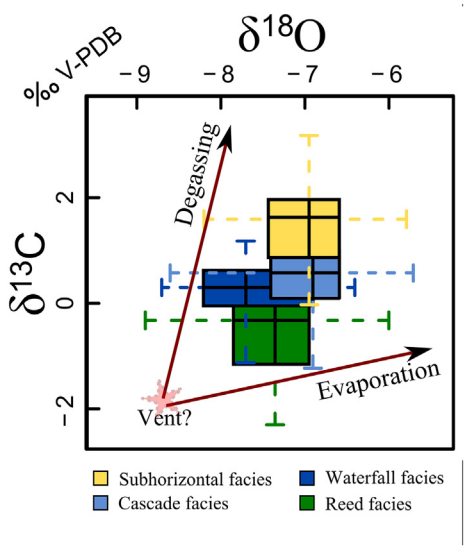

Fig. 9. Combined plot of the $\delta^{18}O$ and $\delta^{13}C$ values for the different facies based on boxplots. Outliers and the Marl-Conglomerate facies have not been plotted. The positive effects of degassing and evaporation are indicated. Degassing is more pronounced for $\delta^{13}C$. Evaporation is more pronounced for $\delta^{18}O$. Based on these trends a presumed vent signature is indicated.

alteration, the carbon and oxygen stable isotopic data do not seem to be dominantly influenced by the diagenetic effects (e.g. Chafetz and Guidry, 2003; Claes et al., 2017b). In active settings of spring-related carbonate precipitation, Sr concentrations decrease downstream from the vent (e.g. Fouke et al., 2000; Kele et al., 2011; Sturchio, 1990). Downstream increase of $\delta^{13}C$ has also widely been reported as a result of continuous enrichment by degassing and evaporation (e.g. Gonfiantini et al., 1968). Based on these observations, the main ancient vent location(s) (highest Sr concentrations of the otherwise rather uniform signature, and the lowest $\delta^{13}C$ values) would be located in the middle of the Killik dome, in line with sedimentological observations (Claes et al., 2015) and present-day topography (Fig. 2) that largely reflects the palaeo-dome topography. The estimated vent location(s) then likely occurred somewhere near the highest point of the dome, which unfortunately is not exposed. Degassing and evaporation, however, would also lead to downstream increasing $\delta^{18}O$ signatures, especially if presumed cooling of the waters would take place (e.g. Fouke et al., 2000). Taking the estimated vent location into account, relatively proximal reed and slightly more distal waterfall facies show relatively depleted $\delta^{18}O$, while the other facies show relatively higher values. The relation between facies and their stable isotope signatures can best be explained by the competition between degassing and evaporation (Fig. 9). The combination of these processes has a positive influence on both the $\delta^{18}O$ and $\delta^{13}C$ signatures (e.g. Pentecost, 2005; Turi, 1986). However, the effect of degassing on $\delta^{13}C$ compared to $\delta^{18}O$ is much more pronounced while, with respect to evaporation, the effect on the $\delta^{18}O$ is more pronounced than that on the $\delta^{13}C$. The waterfall facies are characterised by steep anisopachous and even discontinuous layers that reflect an environment of high turbulence. The high turbulence will lead to fast degassing, that dominates over other processes like evaporation. The result is a relatively higher increase in $\delta^{13}C$ compared to $\delta^{18}O$ (Fig. 9). The cascade facies, formed on smoother slopes, and especially the reed and sub-horizontal facies represent environments where more slowly flowing and even standing waters occurred. In these locations, evaporation will be more pronounced (Fig. 9). In the distal facies, the effect of these processes will be accumulated, resulting in the highest $\delta^{18}O$ and $\delta^{13}C$ values, e.g. in the distal sub-horizontal facies (Fig. 9). In addition, the different extent of disequilibrium precipitation (more pronounced proximal to the vent; Kele et al., 2011) could further accentuate this depositional shift in isotopic signatures.

In conclusion, geochemical trends within a travertine body, can best be explained by the evolution of the fluid characteristics from proximal to distal settings. On the level of lithofacies, their slopes and consequently the turbulence and associated degassing will strongly affect the geochemistry, in line with observations from active settings (e.g. Arenas et al., 2014; Kele et al., 2011). The degassing effect of turbulent water is most pronounced in the steep sloping environment of the waterfall facies. On smoother slopes and particularly in sub-horizontal environments, evaporation will become more dominant. These effects are relatively small on the elemental signatures and more pronounced for stable isotopes. A great potential may lie in the combination of elemental and stable isotope data with clumped isotope geochemistry (e.g. Kele et al., 2015), so that a better environmental constraint on these processes can be acquired.

6. Conclusion

Geochemical analyses can be a strong asset in understanding the depositional history of spring-related travertines. However, choosing the correct laboratorial methodology and statistical data analysis is of crucial importance. This study demonstrates that element concentrations in travertines strongly depend on the digestion methods used. This is particularly explicit for elements related to the non-carbonate fraction. While for weak acids clays will only partly dissolve, stronger acids will lead to a higher elemental contribution due to a more complete dissolution. Even for carbonate phase related elements, an increase in elemental concentrations is observed with increasing acid strength (likely due to the "clay shielding effect"). This implies that elemental concentrations from different mild acid digestion methods cannot be compared to each other, or to results of stronger acid digestion methods. For multiple element comparisons of different travertine systems, a standardised and/or full digestion methodology should be applied, like the 4 acid digestion method used in this study. In order to compare travertine systems independent of external factors acting on the system, only trace elements derived from the carbonate phase should be considered which can be separated based on statistical analysis.

Two important element groups are distinguished. Group I (Ba, Ca, Mg, Na, S and Sr) represents elements related to the carbonate fraction, with elemental variation mainly dependent on the interaction intensity and the concentrations in the element source rock. Group II elements (Al, Fe, Si and Ti) represent the oxides and detrital influx in the system.

Group I elements of the Ballık travertines are interpreted to relate to the interaction of the precipitating waters with the Lycian Nappes, in particular the Kalebogazi Formation, consisting of dolomitised limestones containing evaporites.

The present study points out that dominantly carbonate phase related element signatures (like Sr, S and Ba), in combination with stable isotope data ($\delta^{18}O$ and $\delta^{13}C$), are key geochemical parameters for comparison between travertine geobodies.

Geochemical data reveals elevated Sr concentrations and lowest $\delta^{13}C$ signatures towards the top and centre of the Kıllık dome. Most likely, this indicates main ancient spring locations, in line with sedimentological observations and topography. The distributions of $\delta^{18}O$ and $\delta^{13}C$ are controlled by the cumulative effect and competition between degassing and evaporation.

This study illustrates the application of statistics in understanding and interpreting geochemical trends towards depositional processes. The methodology of this study can be similarly applied to other (even older and subsurface) fossil travertine deposits worldwide. A potentially higher influence of diagenetic effects should, however, be considered. Nonetheless, by integrating elemental data with other geochemical and petrographical data, crucial information on deposition and diagenesis can be acquired. This applies particularly to subsurface reservoirs, where information is limited to borehole data, therefore geochemical data can be decisive in understanding travertine systems.

Acknowledgements

Thanks go to H. Nijs for thin-section preparation. Special thanks to TOTAL, ENI E&P, BG Group and PETROBRAS for funding part of the research. The constructive reviews by M. Gradziński, P.A. Teboul and anonymous reviewers are highly appreciated.

Appendix A. Supplementary data

Supplementary data associated with this article can be found in the online version, at https://doi.org/10.1016/j.sedgeo.2019.04.002. These data include the Google map of the most important areas described in this article.

References

Aitchison, J., 1986. The Statistical Analysis of Compositional Data. Chapman and Hall, Ltd., London, UK, p. 416.
Alçiçek, H., Varol, B., Özkul, M., 2007. Sedimentary facies, depositional environments and palaeogeographic evolution of the Neogene Denizli Basin, SW Anatolia, Turkey. Sediment. Geol. 202, 596–637.
Andrews, J.E., Brasier, A.T., 2005. Seasonal records of climatic change in annually laminated tufas: short review and future prospects. J. Quat. Sci. 20, 411–421.
Arenas, C., Osácar, C., Sancho, C., Vázquez-Urbez, M., Auqué, L., Pardo, G., 2010. Seasonal record from recent fluvial tufa deposits (Monasterio de Piedra, NE Spain): sedimentological and stable isotope data. Geol. Soc. Lond., Spec. Publ. 336, 119–142.
Arenas, C., Vázques-Urbez, M., Pardo, G., Sancho, C., 2014. Sedimentology and depositional architecture of tufas deposited in stepped fluvial systems of changing slope: lessons from the Quaternary Anamaza valley (Iberian Range, Spain). Sedimentology 61, 133–171.
Armengaud, P., Sulpice, R., Miller, A.J., Stitt, M., Amtmann, A., Gibon, Y., 2009. Multilevel analysis of primary metabolism provides new insights into the role of potassium nutrition for glycolysis and nitrogen assimilation in Arabidopsis roots. Plant Physiol. 150, 772–785.
Asta, M.P., Auqué, L.F., Sanz, F.J., Gimeno, M.J., Acero, P., Blasco, M., García-Alix, A., Gómez, J., Delgado-Huertas, A., Mandado, J., 2017. Travertines associated with the Alhama-Jaraba thermal waters (NE, Spain): genesis and geochemistry. Sediment. Geol. 347, 100–116.
Bonny, S.M., Jones, B., 2008. Petrography and textural development of inorganic and biogenic lithotypes in a relict barite tufa deposit at Flybye Springs, NT, Canada. Sedimentology 55, 275–303.
Caboi, R., Cidu, R., Fanfani, L., Zuddas, P., Zuddas, P.P., 1991. Geochemistry of the Funtana Maore travertines (Central Sardinia, Italy). Mineral. Petrogr. Acta 34, 77–93.
Capezzuoli, E., Gandin, A., Pedley, M., 2014. Decoding tufa and travertine (fresh water carbonates) in the sedimentary record: the state of the art. Sedimentology 61, 1–21. https://doi.org/10.1111/sed.12075.
Chafetz, H.S., Guidry, S.A., 2003. Deposition and diagenesis of Mammoth Hot Springs travertine, Yellowstone National Park, Wyoming, U.S.A. Can. J. Earth Sci. 40, 1515–1529.
Cidu, R., Fanfani, L., Zuddas, P., Zuddas, P., 1990. The travertine deposit at Funtana Maore (Central Sardinia, Italy). Geochemistry of the Earth's surface and of mineral formation, 2nd International Symposium, July, 2–8, Aix en Provence, France, pp. 198–200.
Claes, H., Soete, J., Van Noten, K., El Desouky, H., Marques Erthal, M., Vanhaecke, F., Özkul, M., Swennen, R., 2015. Sedimentology, three-dimensional geobody reconstruction and carbon dioxide origin of Pleistocene travertine deposits in the Ballık area (south-west Turkey). Sedimentology 62, 1408–1445.
Claes, H., Marques Erthal, M., Soete, J., Özkul, M., Swennen, R., 2017a. Shrub and pore type classification: petrography of travertine shrubs from the Ballik-Belevi area (Denizli, SW Turkey). Quat. Int. 437 (Part A), 147–163. https://doi.org/10.1016/j.quaint.2016.11.002.
Claes, H., Degros, M., Soete, J., Claes, S., Kele, S., Mindszenty, A., Török, Á., El Desouky, H., Vanhaecke, F., Swennen, R., 2017b. Geobody architecture, genesis and petrophysical characteristics of the Budakalász travertines, Buda Hills (Hungary). Quat. Int. 437 (Part A), 107–128. https://doi.org/10.1016/j.quaint.2016.09.007.
Croci, A., Della Porta, G., Capezzuoli, E., 2016. Depositional architecture of a mixed travertine-terrigenous system in a fault-controlled continental extensional basin (Messinian, Southern Tuscany, Central Italy). Sediment. Geol. 332, 13–39.
Crossey, L.J., Fischer, T.P., Patchett, P.J., Karlstrom, K.E., Hilton, D.R., Newell, D.L., Huntoon, P., Reynolds, A.C., de Leeuw, G.A.M., 2006. Dissected hydrologic system at the Grand Canyon: interaction between deeply derived fluids and plateau aquifer waters in modern springs and travertine. Geology 34, 25–28.
D'Alessandro, W., Giammanco, S., Bellomo, S., Parello, F., 2007. Geochemistry and mineralogy of travertine deposits of the SW flank of Mt. Etna (Italy): relationships with past volcanic and degassing activity. J. Volcanol. Geotherm. Res. 165, 64–70.
De Boever, E., Foubert, A., Oligschlaeger, D., Claes, S., Soete, J., Bertier, P., Özkul, M., Virgone, A., Swennen, R., 2016. Multiscale approach to (micro)porosity quantification in continental spring carbonate facies: Case study from the Cakmak quarry (Denizli, Turkey). Geochem. Geophys. Geosyst. 17 (7), 2922–2939.
De Boever, E., Foubert, A., Lopez, B., Swennen, R., Jaworowski, C., Özkul, M., Virgone, A., 2017. Comparative study of the Pleistocene Cakmak Quarry (Denizli Basin, Turkey) and Modern Mammoth Hot Springs deposits (Yellowstone National Park, USA):

towards an integrated travertine depositional facies model? Quat. Int. 437 (Part A), 129–146. https://doi.org/10.1016/j.quaint.2016.09.011.
Della Porta, G., 2015. Carbonate build-ups in lacustrine, hydrothermal and fluvial settings: comparing depositional geometry, fabric types and geochemical signature. In: Bosence, D.W.J., Gibbons, K.A., Le Heron, D.P., Morgan, W.A., Pritchard, T., Vining, B.A. (Eds.), Microbial Carbonates in Space and Time: Implications for Global Exploration and Production. Geological Society, London, Special Publications 418. https://doi.org/10.1144/SP418.4.
Egozcue, J.J., Pawlowsky-Glahn, V., Mateu-Figueras, G., Barceló-Vidal, C., 2003. Isometric logratio transformations for compositional data analysis. Math. Geol. 35 (3), 279–300.
El Desouky, H., Soete, J., Claes, H., Özkul, M., Vanhaecke, F., Swennen, R., 2015. Novel applications of fluid inclusions and isotope geochemistry in unravelling the genesis of fossil travertine systems. Sedimentology 62, 27–56.
Fairchild, I.J., Treble, P.C., 2009. Trace elements in speleothems as recorders of environmental change. Quat. Sci. Rev. 28, 449–468.
Filzmoser, P., Hron, K., 2009. Correlation analysis for compositional data. Math. Geosci. 41, 905–919.
Filzmoser, P., Hron, K., Reimann, C., 2009. Principal component analysis for compositional data with outliers. Environmetrics 20, 621–632.
Ford, T.D., Pedley, H.M., 1996. A review of tufa and travertine deposits of the world. Earth-Sci. Rev. 41, 117–175.
Fouke, B.W., Farmer, J.D., Des Marais, D.J., Pratt, L., Sturchio, N.C., Burns, P.C., Discipulo, M.K., 2000. Depositional facies and aqueous-solid geochemistry of travertine-depositing hot springs (Angel Terrace, Mammoth Hot Springs, Yellowstone National Park, U.S.A.). J. Sediment. Res. 70, 565–585.
Frery, E., Gratier, J.-P., Ellouz-Zimmerman, N., Deschamps, P., Blamart, D., Hamelin, B., Swennen, R., 2017. Geochemical transect through a travertine mount: a detailed record of CO2-enriched fluid leakage from Late Pleistocene to present-day – Little Grand Wash fault (Utah, USA). Quat. Int. 437 (Part A), 98–106. https://doi.org/10.1016/j.quaint.2016.09.035.
Garnett, E.R., Andrews, J.E., Preece, R.C., Dennis, P.F., 2004. Climatic change recorded by stable isotopes and trace elements in a British Holocene tufa. J. Quat. Sci. 19, 251–262.
Gleyzes, C., Tellier, S., Astruc, M., 2002. Fractionation studies of trace elements in contaminated soils and sediments: a review of sequential extraction procedures. Trends Anal. Chem. 21, 451–467.
Gonfiantini, R., Panichi, C., Tongiorgi, E., 1968. Isotopic disequilibrium in travertine deposition. Earth Planet. Sci. Lett. 5, 55–58.
Gradzinski, M., Hercman, H., Jaskiewicz, M., Szczurek, S., 2013. Holocene tufa in the Slovak Karst: facies, sedimentary environments and depositional history. Geol. Q. 57 (4), 769–788.
Gündoğan, İ., Helvacı, C., Sözbilir, H., 2008. Gypsiferous carbonates at Honaz Dağı (Denizli): first documentation of Triassic gypsum in western Turkey and its tectonic significance. J. Asian Earth Sci. 32, 49–65.
Howard, J., Vandenbrink, W., 1999. Sequential extraction analysis of heavy metals in sediments of variable composition using nitrilotriacetic acid to counteract resorption. Environ. Pollut. 106, 285–292.
Ihlenfeld, C., Norman, M., Gagan, M., 2003. Climatic significance of seasonal trace element and stable isotope variations in a modern freshwater tufa. Geochim. Cosmochim. Acta 67, 2341–2357.
Irion, G., Müller, G., 1968. Mineralogy, petrology and chemical composition of some calcareous tufa from the Schwälbische Alb, Germany. In: Müller, G., Freidman, G.M. (Eds.), Carbonate Sedimentology in Central Europe. Springer, New York, pp. 157–171.
Kallis, P., Bleich, K.E., Stahr, K., 2000. Micromorphological and geochemical characterization of Tertiary 'freshwater carbonates' locally preserved north of the edge of the Miocene Molasse Basin (SW Germany). Catena 41, 19–42.
Kampman, N., Burnside, N.M., Shipton, Z.K., Chapman, H.J., Nicholl, J.A., Ellam, R.M., Bickle, M.J., 2012. Pulses of carbon dioxide emissions from intracrustal faults following climatic warming. Nat. Geosci. 5, 352–358.
Kele, S., Demény, A., Siklósy, Z., Németh, T., Tóth, M., Kovács, M.B., 2008. Chemical and stable isotope composition of recent hot-water travertines and associated thermal waters, from Egerszalók, Hungary: depositional facies and non-equilibrium fractionation. Sediment. Geol. 211, 53–72.
Kele, S., Özkul, M., Fórizs, I., Gökgöz, A., Baykara, M.O., Alçiçek, M.C., Németh, T., 2011. Stable isotope geochemical study of Pamukkale travertines: new evidences of low-temperature non-equilibrium calcite-water fractionation. Sediment. Geol. 238, 191–212.
Kele, S., Breitenbach, S.F.M., Capezzuoli, E., Meckler, A.N., Ziegler, M., Millan, I.M., Kluge, T., Deák, J., Hanselmann, K., John, C.M., Yan, H., Liu, Z., Bernasconi, S.M., 2015. Temperature dependence of oxygen- and clumped isotope fractionation in carbonates: a study of travertines and tufas in the 6–95 °C temperature range. Geochim. Cosmochim. Acta 168, 172–192.
Khatib, S., Rochette, P., Alçiçek, M.C., Lebatard, A.-E., Demory, F., Saos, T., 2014. Études stratigraphique, sédimentologique et paléomagnétique des travertins de Kocabaş, Bassin de Denizli, Anatolie, Turquie, contenant des restes fossiles quaternaires. Anthropologie 1–18.
Kynclova, P., Filzmoser, P., Hron, K., 2016. Compositional biplots including external non-compositional variables. Statistics 50 (5), 1132–1148.
Lebatard, A.-E., Alçiçek, M.C., Rochette, P., Khatib, S., Vialet, A., Boulbes, N., Bourlès, D.L., Demory, F., Guipert, G., Mayda, S., Titov, V.V., Vidal, L., de Lumley, H., 2014. Dating the Homo erectus bearing travertine from Kocabas (Denizli, Turkey) at at least 1.1 Ma. Earth Planet. Sci. Lett. 390, 8–18.
Leybourne, M.I., Betcher, R.N., McRitchie, W.D., Kaszycki, C.A., Boyle, D.R., 2009. Geochemistry and stable isotopic composition of tufa waters and precipitates from the Interlake Region, Manitoba, Canada: constraints on groundwater origin, calcitization, and tufa formation. Chem. Geol. 260, 221–233.
Lovrenčić Mikelić, I., Oreščanin, V., Barišić, D., 2013. Distribution and origin of major, minor, and trace elements in sediments and sedimentary rocks of the Kaštela Bay (Croatia) coastal area. J. Geochem. Explor. 128, 1–13.
Mallick, R., Frank, N., 2002. A new technique for precise uranium-series dating of travertine micro-samples. Geochim. Cosmochim. Acta 66 (24), 4261–4272.
McArthur, J.M., Howarth, R.J., 2004. Sr-Isotope Stratigraphy in a Geologic Time Scale.
Minissale, A., 2004. Origin, transport and discharge of CO_2 in central Italy. Earth-Sci. Rev. 66, 89–141.
Minissale, A., Kerrick, D.M., Magro, G., Murrell, M.T., Paladini, M., Rihs, S., Sturchio, N.C., Tassi, F., Vaselli, O., 2002. Geochemistry of Quaternary travertines in the region north of Rome (Italy): structural, hydrologic and paleoclimatic implications. Earth Planet. Sci. Lett. 203, 709–728.
Mohammadi, Z., Claes, H., Cappezuoli, E., Mozafari, M., Soete, J., Aratman, C., Swennen, R., 2019. Lateral and vertical variation in sedimentology and geochemistry of subhorizontal laminated travertines (Cakmak quarry, Denizli Basin, Turkey). Quat. Int. https://doi.org/10.1016/j.quaint.2018.11.041.
Özkul, M., Kele, S., Gökgöz, A., Shen, C.-C., Jones, B., Baykara, M.O., Fórizs, I., Németh, T., Chang, Y.-W., Alçiçek, M.C., 2013. Comparison of the Quaternary travertine sites in the Denizli extensional basin based on their depositional and geochemical data. Sediment. Geol. 294, 179–204.
Pavlovic, G., Prohic, E., Miko, S., Tibljas, D., 2002. Geochemical and petrographic evidence of meteoric diagenesis in tufa deposits in Northern Dalmatia (Zrmanja and Krupa rivers, Croatia). Facies 46, 27–34.
Pedley, H.M., 1990. Classification and environmental models of cool freshwater tufas. Sediment. Geol. 68, 143–154.
Pentecost, A., 1993. British travertines: a review. Proc. Geol. Assoc. 104, 23–39.
Pentecost, A., 1999. The origin and development of the travertines and associated thermal waters at Matlock Bath, Derbyshire. Proc. Geol. Assoc. 110, 217–232.
Pentecost, A., 2005. Travertine. Springer-Verlag, Berlin Heidelberg (445 pp.).
Pisarskii, B.I., Konev, A.A., Levi, K.G., Delvaux, D., 1998. Carbon dioxide-bearing alkaline hydrotherms and strontium-bearing travertines in the Songwe River Valley. Russ. Geol. Geophys. 39, 941–948.
R core team, 2013. R: A language and Environment for Statistical Computing. R Foundation for statistical computing, Vienna http://www.r-project.org.
Rainey, D.K., Jones, B., 2007. Rapid cold water formation and recrystallisation of relict bryophyte tufa at the Fall Creek cold springs, Alberta, Canada. Can. J. Earth Sci. 44, 889–909.
Rauch, H., White, W., 1977. Dissolution kinetics of carbonate rocks. 1. Effects of lithology on dissolution rate. Water Resour. Res. 13, 381–394.
Renaut, R.W., Owen, R.B., Jones, B., Tiercelin, J.-J., Tarits, C., Ego, J.K., Konhauser, K.O., 2013. Impact of lake-level changes on the formation of thermogene travertine in continental rifts: evidence from Lake Borgoria, Kenya Rift Valley. Sedimentology 60, 428–468.
Rendell, P.S., Batley, G.E., Cameron, A.J., 1980. Adsorption as a control of metal concentrations in sediment extracts. Environ. Sci. Technol. 14, 314–318.
Rodríguez-Berriguete, Á., Alonso-Zarza, A.M., Martín-García, R., 2017. Diagenesis of continental carbonate country rocks underlying surficial travertine spring deposits. Quat. Int. 437 (Part A), 4–14. https://doi.org/10.1016/j.quaint.2016.09.013.
Ronchi, P., Cruciani, F., 2015. Continental carbonates as a hydrocarbon reservoir, an analog case study from the travertine of Saturnia, Italy. AAPG Bull. 99 (4), 711–734.
Ross, D.J., 1991. Botryoidal high-magnesium calcite marine cements from the Upper Cretaceous of the Mediterranean region. J. Sediment. Res. 61 (3), 349–353.
Salminen, R., Reeder, S., De Vivo, B., Demetriades, A., Pirc, S., Batista, M.J., Marsina, K., Ottesen, R.T., O'Connor, P.J., Bidovec, M., Lima, A., Siewers, U., Smith, B., Taylor, H., Shaw, R., Salpeteur, I., Gregorauskiene, V., Halamic, J., Slaninka, I., Lax, K., Gravesen, P., Birke, M., Breward, N., Ander, E.L., Jordan, G., Duris, M., Klein, P., Locutura, J., Bellan, A., Pasieczna, A., Lis, J., Mazreku, A., Gilucis, A., Heitzmann, P., Klaver, G., Petersell, V., 2006. Geochemical atlas of Europe. In: De Vos, W., Tervainen, T. (Eds.), Part 2 - Interpretation of Geochemical Maps, Additional Tables, Figures, Maps, and Related Publications. Geological Survey of Finland.
Sant'Anna, L.G., Riccomini, C., Rodrigues-Francisco, B.H., Sial, A.N., Carvalho, M.D., Moura, C.A.V., 2004. The Paleocene travertine system of the Itaboraí basin, Southeastern Brazil. J. S. Am. Earth Sci. 18, 11–25.
Simsek, S., 1984. Geology and geothermal energy potential of the Denizli-Kizildere-Tekkehamam-Tosunlar-Buldan-Yenice area. Ankara, Bulletin of the Mineral Research and Exploration (MTA), Scientific Report 85.
Soete, J., Kleipool, L.M., Claes, H., Claes, S., Hamaekers, H., Kele, S., Özkul, M., Foubert, A., Reijmer, J.J.G., Swennen, R., 2015. Acoustic properties in travertines and their relation to porosity and pore types. Mar. Pet. Geol. 59, 320–335.
Sturchio, N.C., 1990. Radium isotopes, alkaline earth diagenesis, and age determination of travertine from Mammoth Hot Springs, Wyoming, U.S.a. Appl. Geochem. 5, 631–640.
Sun, S., 1990. Geology of the region between Denizli and Usak and lignite potentials. Ankara, Bulletin of the Mineral Research and Exploration (MTA), Scientific Report.
Swennen, R., Viaene, W., Bouckaert, J., Simakov, K.V., Van Oyen, P., 1986. Lithogeochemistry of Upper Famennian-Tournaisian strata in the Omolon area (NE-USSR) and its implications. Ann. Soc. Geol. Belg. 109, 249–261.
Teboul, P.A., Durlet, C., Gaucher, E.C., Virgone, A., Girard, J.P., Curie, J., Lopez, B., Camoin, G.F., 2016. Origins of elements building travertine and tufa: new perspectives provided by isotopic and geochemical tracers. Sediment. Geol. 334, 97–114.
Török, Á., Mindszenty, A., Claes, H., Kele, S., Fodor, L., Swennen, R., 2017. Geobody architecture of continental carbonates: "Gazda" travertine quarry (Süttő, Gerecse Hills, Hungary). Quat. Int. 437 (Part A), 164–185. https://doi.org/10.1016/j.quaint.2016.09.030.
Turi, B., 1986. Stable isotope geochemistry of travertines. In: Fritz, B.P., Fontes, J.C. (Eds.), Handbook of Environmental Isotope Geochemistry. Elsevier, Amsterdam, pp. 207–235.

Van den Boogaert, K.G., Tolosano-Delgado, R., 2013. Analyzing Compositional Data with R, Use R! Berlin Heidelberg, Springer-Verlag, pp. 13–50 https://doi.org/10.1007/978-3-642-36809-7_2.

Van Noten, K., Claes, H., Soete, J., Foubert, A., Özkul, M., Swennen, R., 2013. Fracture networks and strike – slip deformation along reactivated normal faults in Quaternary travertine deposits, Denizli Basin, western Turkey. Tectonophysics 588, 154–170.

Van Noten, K., Topal, S., Baykara, M.O., Özkul, M., Claes, H., Aratman, C., Swennen, R., 2019. Pleistocene-Holocene tectonic reconstruction of the Ballik travertine (Denizli Graben, SW Turkey): (de)formation of large travertine geobodies at intersecting grabens. J. Struct. Geol. 118, 114–134.

Wang, H., Yan, H., Liu, Z., 2014. Contrasts in variations of the carbon and oxygen isotopic compositions of travertines formed in pools and a ramp stream at Huanglong Ravine, China: implications for paleoclimatic interpretations. Geochim. Cosmochim. Acta 125, 34–48.

Yan, H., Sun, H., Liu, Z., 2012. Equilibrium vs. kinetic fractionation of oxygen isotopes in two low-temperature travertine-depositing systems with differing hydrodynamic conditions Baishuitai, Yunnan, SW China. Geochim. Cosmochim. Acta 95, 63–78.